

Dependence of Modulation Amplitude on Electron Density in Unidirectional Lateral Superlattices: The Effect of the Thickness of the Two-dimensional Electron Gas

Akira ENDO* and Yasuhiro IYE

Institute for Solid State Physics, University of Tokyo, 5-1-5 Kashiwanoha, Kashiwa, Chiba 277-8581

The amplitude V_0 of unidirectional periodic potential modulation introduced by a surface grating into a two-dimensional electron gas (2DEG) formed at AlGaAs/GaAs heterointerface is measured as a function of electron density n_e by analyzing commensurability oscillation of the magnetoresistance. The electron density is varied either by applying a bias to a metallic back gate or by illumination. The amplitude decreases with increasing density, with the rate $|dV_0/dn_e|$ roughly an order of magnitude larger for the former method. The result is interpreted in terms of the rate, $dE_1/d(\delta E_c)$, of the change in the first subband level E_1 in response to the variation of the conduction-band edge δE_c above the heterointerface. The rate crucially depends on the thickness of the 2DEG.

KEYWORDS: two-dimensional electron gas, AlGaAs/GaAs single heterostructure, potential modulation, lateral superlattice, electron density, thickness, back gate, illumination, commensurability oscillation

1. Introduction

A two-dimensional electron gas (2DEG) formed at $\text{Al}_x\text{Ga}_{1-x}\text{As}/\text{GaAs}$ heterointerface has been the basis of a multitude of experimental studies for low-dimensional electron systems. The devices for such experiments are produced by processing the surface of the 2DEG wafers by micro- (or nano-) fabrication techniques: depositing patterned gates or etching off part of the wafers, thereby introducing electrostatic potential modulation or confining electrons to smaller areas.¹ The modern nanofabrication technology grants fine control of the lateral dimensions of the patterns down to the length scale less than 100 nm, limited only by the depth of 2DEG plane from the surface. In contrast to the high controllability of the lateral length scale, the energy scale involved, the magnitude of the potential modulation, allows much poorer management. The amplitudes are often adjusted, chiefly on empirical basis, only for a certain particular purpose, e.g., depleting electrons underneath the metallic gate by applying negative bias. It is usually not easy even to measure, much less to precisely adjust, the amplitude of the modulation for generic cases. An important exception is when the modulation possesses a unidirectional periodicity. The *unidirectional lateral superlattice* (ULSL) reveals the amplitude V_0 of the modulation through the amplitude of the commensurability oscillation (CO), the magnetoresistance oscillation resulting from the commensurability between the period a of the modulation and the cyclotron radius R_c .²

In the present paper, we report the behavior of the modulation amplitude when the electron density n_e is varied, in pursuit of better quantitative understanding of the energy scale relevant in the study of low-dimensional electron systems. The amplitude V_0 is measured using CO of ULSL. We shed light on the effect of finite thickness of the 2DEG wave function, which is often neglected in the first order approximation but nevertheless can be

of vital importance for phenomena in which electron-electron interaction plays a crucial role.³ In a ULSL, a grating that introduces potential modulation to the 2DEG plane is placed on the front surface. Therefore, it is clear that a metallic uniform front gate, a standard device to vary n_e , cannot be employed without heavily affecting the modulation amplitude. We have instead made use of metallic gate on the backside of the wafer, or illumination by light emitting diode (LED). Naively, one would expect the modulation amplitude to be basically insensitive to the back gate, since the grating and the back gate, being situated on the opposite side of the 2DEG, is expected to cause minimal crosstalk. It turns out, however, that the amplitude varies substantially in response to the back gate, much more pronounced than when n_e is modified by illumination. The large variation is ascribed to the modification in the width of the well confining the electrons in the vertical direction, hence to the thickness of the 2DEG wave function. The experimental methods and results are described in §2 and 3, respectively. The interpretation of the experimental results is discussed in detail in §4, followed by concluding remarks in §5.

2. Experimental

Two ULSL samples with differing periods were prepared from the same $\text{Al}_x\text{Ga}_{1-x}\text{As}/\text{GaAs}$ ($x=0.33$) single-heterostructure (SH) 2DEG wafer having the mobility $\mu \simeq 70 \text{ m}^2/\text{Vs}$ and electron density $n_e \simeq 2 \times 10^{15} \text{ m}^{-2}$ at $T=4.2 \text{ K}$. The structure of the wafer was (from the front surface) 10 nm GaAs cap layer, 40 nm Si-doped ($N_{\text{Si}}=2 \times 10^{24} \text{ m}^{-3}$) $\text{Al}_x\text{Ga}_{1-x}\text{As}$ layer, 40 nm undoped $\text{Al}_x\text{Ga}_{1-x}\text{As}$ spacer layer, and 1 μm GaAs layer with 2DEG channel residing near the interface to the upper layer. As depicted in Fig. 1(c), a pair of Hall bars, $44 \times 16 \mu\text{m}^2$, were defined in series by wet-etching; one of these was further processed into ULSL and the other was reserved as reference. The potential modulation was intro-

*E-mail address: akrendo@issp.u-tokyo.ac.jp

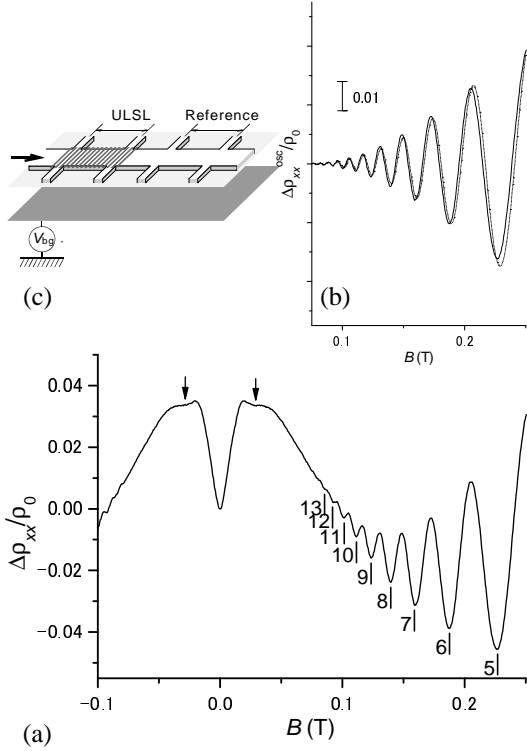


Fig. 1. (a) A typical magnetoconductance trace showing PMR and CO (taken at 4.2 K). (The example is for sample B at $n_e=2.2\times 10^{15} \text{ m}^{-2}$). Arrows mark the position of B_{inf} . Minima in CO are labeled by their index numbers. (b) Oscillatory part of CO, obtained by subtracting the slowly varying background. The dotted curve represents a fit to eq. (1). (c) Schematic drawing of the sample.

duced employing strain-induced piezoelectric effect⁴ by a grating of high-resolution negative electron-beam resist⁵ placed on the front surface.⁶ The periods are $a=161$ and 138 nm for samples A and B, respectively. A uniform metallic (gold) gate was deposited on the rear side of the wafer after thinning the wafer from 0.3 mm down to about 0.1 mm by wet-etching in order to enhance the effectiveness of the back gate. No signs of deterioration in the mobility were observed after these processing.⁷ The electron density varies, by Δn_{bg} , in response to the bias V_{bg} applied to the back gate. From the rate $d(\Delta n_{\text{bg}})/dV_{\text{bg}}=5.0\times 10^{-3}$ and 4.1×10^{-3} in $10^{15} \text{ m}^{-2}/\text{V}$, the distance of 2DEG plane from the back gate was estimated to be $d_{\text{bg}}=140$ and $170 \text{ }\mu\text{m}$ by a simple capacitance model $e\Delta n_{\text{bg}}=(\epsilon_0\epsilon/d_{\text{bg}})V_{\text{bg}}$ for samples A and B, respectively.

Figure 1(a) shows a typical magnetoconductance trace of our ULSL, taken by standard low-frequency ac lock-in technique at 4.2 K. The trace exhibits CO as well as positive magnetoresistance⁸ (PMR) emanating from $B=0$. The amplitude V_0 of the unidirectional periodic potential modulation⁹ $V_{\text{mod}}(x) = V_0 \cos(qx)$ with $q = 2\pi/a$, can be deduced from the amplitude of CO. In order to obtain accurate quantitative value, however, care should be taken of the impurity scattering that scatters electrons out of the cyclotron orbit before completing a cycle. Such scattering reduces the CO amplitude, more effec-

tively for smaller B where cyclotron circumference $2\pi R_c$ is large, and can lead to the underestimation of V_0 if the standard prescription^{10,11} is used for the analysis. The present authors have shown⁶ that the scattering can be well accounted for by the inclusion of an additional factor $A(\pi/\mu_W B)$ in the formula as,

$$\frac{\Delta\rho_{xx}^{\text{osc}}}{\rho_0} = A\left(\frac{\pi}{\mu_W B}\right) A\left(\frac{T}{T_a}\right) \times \frac{1}{2\sqrt{2\pi}} \frac{1}{\Phi_0 \mu_B^{*2}} \frac{\mu^2}{a} \frac{V_0^2}{n_e^{3/2}} |B| \sin\left(2\pi \frac{2R_c}{a}\right), \quad (1)$$

where $A(x)=x/\sinh(x)$, $k_B T_a=(1/2\pi^2)(ak_F/2)\hbar\omega_c$ with $\omega_c=eB/m^*$, $\Phi_0=h/e$, $\mu_B^*\equiv e\hbar/2m^*$, and $R_c=\hbar k_F/e|B|$ with $k_F=(2\pi n_e)^{1/2}$ the Fermi wave number. As shown in Fig. 1(b), the oscillatory part of the magnetoconductance can be fitted, with μ_W and V_0 as fitting parameters, to eq. (1) very well. The parameter μ_W describes the degree of decay of CO amplitude with decreasing B , and was shown to be able to be identified with⁶ the single-particle or quantum mobility μ_Q deduced from the analysis of the decay of Shubnikov-de Haas oscillation¹² in the adjacent reference plain Hall bar. An alternative way to deduced V_0 is provided by the analysis of PMR. The present authors have recently pointed out¹³ that inflection points B_{inf} at which curvature of the magnetoconductance changes from concave down to concave up, as pointed by the arrows in Fig. 1(a), can be found on the PMR when V_0 is small enough, and B_{inf} corresponds to the extinction field,

$$B_e = \frac{2\pi m^* V_0}{ae\hbar k_F}, \quad (2)$$

where streaming orbits, the orbit of electron confined in a single period, cease to exist. The values of V_0 deduced by this second method agree very well with those drawn using eq. (1), confirming that reliable values are obtained.

3. Results

Figure 2(a) shows V_0 obtained using eq. (1) from the amplitude of CO for samples A and B, plotted as a function of n_e . The electron density n_e is varied either by back-gate voltages (solid symbols) or by illumination with an infrared LED resorting to the persistent photoconductivity effect (open symbols). The ratio of V_0 to the Fermi energy E_F ranges from 2 to 4% for sample A, and 1 to 2% for sample B. It can clearly be seen that V_0 decreases with increasing n_e for both samples. The rate of the decrease dV_0/dn_e is nearly an order of magnitude larger when n_e is varied by the back gate. Although V_0 of sample A is much larger than that of sample B,¹⁴ the relative change, V_0 normalized by the value at $n_e=2.0\times 10^{15} \text{ m}^{-2}$, shows almost the same behavior for both samples, as demonstrated in Fig. 2(b).

Decrease of the modulation amplitude V_0 in response to the increase in n_e by a back gate was also reported by Soibel *et al.*¹⁵ As will be detailed in the next section, the decrease cannot be ascribed to the screening by 2DEG, which is independent of n_e unless a is less than the half of the Fermi wavelength λ_F . In the case of ref. 15, V_0 , hence the ratio V_0/E_F , is roughly an order of magnitude larger than those of our samples. The authors of

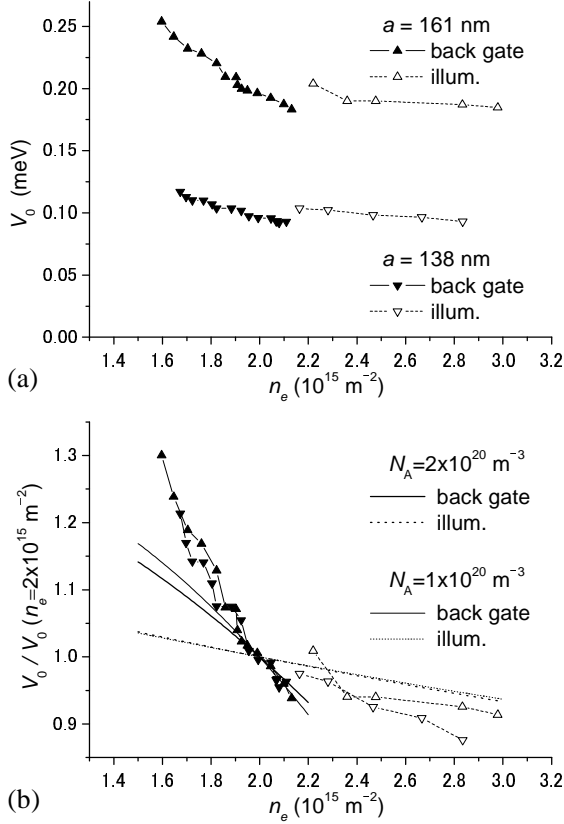


Fig. 2. (a) Amplitudes V_0 of potential modulation, deduced from CO at 4.2K using eq. (1), plotted as a function of the electron density n_e . Solid and open symbols indicate that the densities were varied by the back gate or by illumination, respectively. Upward and downward triangles represent samples A ($a=161 \text{ nm}$) and B ($a=138 \text{ nm}$), respectively. (b) Amplitudes normalized by interpolated (n_e back-gate controlled) or extrapolated (n_e illumination controlled) values at $n_e=2.0 \times 10^{15} \text{ m}^{-2}$. Calculated curves simulating the variation of n_e by the back gate and illumination are shown by solid and dotted curves, respectively, for $N_A=1.0$ and $2.0 \times 10^{20} \text{ m}^{-3}$ as thin and thick curves, respectively. (See text for details.)

ref. 15 pointed out that their V_0 is not small enough to be treated within the standard framework of the screening theory; they claimed that alteration of the 2DEG density of state by their large V_0 should be taken into consideration. Obviously, such explanation does not apply to our samples having V_0 of only a few percent of E_F . In the next section, we will describe our interpretation of the behavior of V_0 caused by the change of n_e .

4. Discussion

4.1 Screening

We start by examining the effect of screening. In the Lindhard formula, the dielectric constant for an ideal zero-thickness 2DEG is given by^{16,17} $\epsilon_0 \epsilon_{\text{es}}(q)$ with $\epsilon_0=8.85 \times 10^{-12} \text{ F/m}$ the permittivity of the vacuum, ϵ the relative dielectric constant of the host crystal ($\epsilon=13.18$ for GaAs), and

$$\epsilon_{\text{s}}(q) = 1 + \frac{2}{a_B^* q} \left\{ 1 - \text{Re} \left[\sqrt{1 - \left(\frac{2k_F}{q} \right)^2} \right] \right\}, \quad (3)$$

expressing the screening by the 2DEG. $a_B^*=4\pi\epsilon_0\epsilon\hbar^2/m^*e^2$ represents the effective Bohr radius for the host material (10.4 nm for GaAs). In eq. (3), only the last term depends on n_e , which disappears at $q < 2k_F$. Namely, the change in n_e , *per se*, does not affect the screening for $a \geq \lambda_F/2$, where $\epsilon_{\text{s}}(q)$ equals $\epsilon_{\text{TF}}(q)=1 + 2/a_B^*q$ calculated by Thomas-Fermi approximation. For the range $n_e=1.5\text{--}3.0 \times 10^{15} \text{ m}^{-2}$ of the electron density investigated in the present study, $\lambda_F=45\text{--}65 \text{ nm}$, and therefore, the screening by 2DEG of our potential modulation $V_{\text{mod}}(x)$ will not depend on n_e . For realistic 2DEG with finite thickness, $\epsilon_{\text{TF}}(q)$ should be slightly modified to include the form factor $F(q)$:

$$\epsilon_{\text{TF}}(q) = 1 + \frac{2}{a_B^* q} F(q). \quad (4)$$

The form factor is defined as^{18–20}

$$\begin{aligned} F(q) &\equiv 2q \int \frac{dk}{2\pi} \frac{\tilde{f}(k)\tilde{f}(-k)}{q^2 + k^2} \\ &= \iint dz dz' f(z)f(z') \exp(-q|z - z'|), \end{aligned} \quad (5)$$

using the Fourier transform $\tilde{f}(k)$ of the (normalized) electron distribution function $f(z)=|\psi(z)|^2$ in the z direction, the direction normal to the 2DEG plane. $\psi(z)$ designates the envelope function of the electron wave function $\psi(z)\exp[i(k_x x + k_y y)]$. It can readily be seen that $F(q)=1$ for $f(z)=\delta(z)$, an ideal 2DEG. As a rule of thumb, $F(q)$ decreases when $f(z)$ is widely spread: the screening is less effective for thicker 2DEG. For example, for Fang-Howard wave function^{16,21} $\psi_{\text{FH}}(z)=\Theta(z)(b^3/2)^{1/2}z \exp(-bz/2)$, $F(q)=b(8b^2 + 9bq + 3q^2)/8(b+q)^3=1 - 15/8(q/b) + 3(q/b)^2 + O[(q/b)^3]$. Here, $\Theta(z)$ represents the unit step function. The variational parameter b , given by $b=[48\pi(n_{\text{depl}} + 11n_e/32)/a_B^*]^{1/3}$ with n_{depl} the depletion charge, is inversely proportional to the thickness of the wave function [rms thickness $(\langle z^2 \rangle - \langle z \rangle^2)^{1/2}=3^{1/2}/b$], and therefore $F(q)$ decreases with increasing thickness.

The thickness of 2DEG varies with n_e , and therefore the change in n_e can, in principle, alter the modulation amplitude seen by the electrons through the change in the screening. However, it is obvious that this thickness-mediated change in the screening is unable to explain our $V_0 - n_e$ relationship even in the qualitative level. As we will see in the next section (Fig. 5(a)), the rms thickness decreases with increasing n_e , leading the screening to be more effective thus letting V_0 smaller, if n_e is varied by illumination (or by a front gate). However, it is the other way around when the back gate is used: the thickness, hence V_0 , is expected to increase with increasing n_e , at variance with the experiment. Furthermore, it can be demonstrated that the change in $\epsilon_{\text{TF}}(q)$ is too small, roughly 1% at most, by evaluating eq. (5) using numerically calculated $\psi(z)$ that will be described in the next subsection. The observed V_0 vs n_e requires a mechanism other than the screening for its explanation. In what follows, we neglect altogether the change in $\epsilon_{\text{TF}}(q)$ by n_e .

4.2 The conduction-band edge and the subband level

For the range of n_e and the temperature, 4.2 K, considered in the present paper, electrons occupy only the lowest subband in the confinement potential. The potential modulation seen by the electrons is the spatial variation of this subband level, E_1 , with respect to the Fermi level. By contrast, it is the conduction-band edge E_c , not E_1 , that is modified by the external devices to introduce potential modulation (a grating placed on the surface in the present study); they do not directly couple to E_1 . The distinction is not important when the two energy levels shift in parallel, which will be approximately the case for 2DEG in a narrow quantum well. In general, however, the shift in E_1 does not necessarily exactly follow the shift in E_c . The subband level E_1 , hence the conversion rate $dE_1/d(\delta E_c)$ from the shift δE_c in the conduction-band edge, evaluated just above the heterointerface where wave function of the electron vanishes, to E_1 , is dependent on the width or the profile of the confinement potential $V(z)$ in which the subband is formed. In $\text{Al}_x\text{Ga}_{1-x}\text{As}/\text{GaAs}$ SH 2DEG, electrons themselves and the back-gate voltages are important ingredients for determining the profile of $V(z)$, as we will see below. Therefore, $dE_1/d(\delta E_c)$ varies with electron density or back-gate conditions. In what follows, we demonstrate by numerical simulation using simplified model that the observed variation of V_0 by the back gate or illumination is mainly attributable to the concomitant change in $dE_1/d(\delta E_c)$.

The potential well confining the electrons is given by,^{22,23}

$$V(z) = V_b\Theta(-z) + (-e)\phi(z) + V_{xc}(z). \quad (6)$$

Here, we define $z=0$ as the heterointerface, and the z -axis points down into the substrate ($z<0$: $\text{Al}_x\text{Ga}_{1-x}\text{As}$ and $z>0$: GaAs). $V(z)$ is comprised of the band discontinuity $V_b\Theta(-z)$ at the heterointerface ($V_b=292$ meV for $x=0.33$ at 4.2 K) and the electrostatic potential $(-e)\phi(z)$ originating from the ionized donor (Si) at doped $\text{Al}_x\text{Ga}_{1-x}\text{As}$ layer, remnant background impurities, as well as the electrons themselves (the Hartree term). The exchange-correlation effects, the effects of electron-electron interaction beyond the Hartree approximation, is also taken into account as parameterized potential²⁴ $V_{xc}(z)$ after Stern and Sarma,²³

$$V_{xc}(z) = - \left[1 + 0.7734 \frac{r_s}{21} \ln \left(1 + \frac{21}{r_s} \right) \right] \frac{2}{(4/9\pi)^{1/3} \pi r_s} \text{Ry}^*, \quad (7)$$

where

$$r_s \equiv r_s(z) = \left[\frac{4}{3} \pi a_B^*{}^3 n_e |\psi(z)|^2 \right]^{-1/3} \quad (8)$$

and $\text{Ry}^* = e^2/8\pi\epsilon_0\epsilon_B a_B^*$ the effective Rydberg energy (5.2 meV for GaAs). The electrostatic potential is determined by solving the Schrödinger equation,

$$-\frac{\hbar^2}{2m^*} \frac{d^2}{dz^2} \psi(z) + V(z)\psi(z) = E_1\psi(z) \quad (9)$$

and Poisson's equation,

$$\frac{d^2}{dz^2} \phi(z) = -\frac{(-e)}{\epsilon_0\epsilon} [n_e |\psi(z)|^2 + N_A \Theta(z)] \quad (10)$$

self-consistently. Here we have made several types of simplifications: the difference in the effective mass and dielectric constant between the two materials is neglected and those for GaAs ($m^*=0.067m_e$ and $\epsilon=13.18$) are used throughout, and accordingly the image potential energy is ignored; possible atomic-scale smooth grading of the band discontinuity at the interface considered in ref. 23 is neglected; the background residual impurity N_A is taken into account only at $z>0$.²⁵ These approximations are expected not to affect the present argument very much. In GaAs -based materials grown in the modern molecular beam epitaxy (MBE) machines, it is known that the residual impurity is mainly composed of carbon that is unintentionally incorporated into the crystal. In GaAs , the carbon works as an acceptor, whose density N_A in the particular 2DEG wafer used in the present study is difficult to know. It can be estimated, however, to be close to $1.7 \times 10^{20} \text{ m}^{-3}$ inferred from Hall measurement for nominally undoped GaAs bulk crystal grown slightly before the present 2DEG wafer was grown, using the identical MBE chamber. Therefore we use N_A near this value for calculations.

The effects of the ionized donor, the background impurity, and the back gate are taken into account as suitable boundary conditions. The slope of the electrostatic potential just below the 2DEG, i.e., where $|\psi(z)|^2$ vanishes at $\langle z \rangle < z \ll z_{\text{depl}}$ (with $\langle z \rangle$ and z_{depl} denoting the average position of the wave function and the depletion layer thickness, respectively), is determined by the electric field due to the depletion charge n_{depl} and the slope by the back gate. We parameterize the effect of the back gate by the change in the electron density Δn_{bg} induced by applying the back-gate voltage V_{bg} ; $e\Delta n_{\text{bg}} = (\epsilon_0\epsilon/d_{\text{bg}})V_{\text{bg}}$ as defined before. Thus, by Gauss's theorem, $-d\phi/dz = (-e/\epsilon_0\epsilon)(n_{\text{depl}} - \Delta n_{\text{bg}})$. The slope just above the 2DEG (where $|\psi(z)|^2$ vanishes at $-d_{\text{sp}} \ll z < 0$, with $d_{\text{sp}}=40$ nm representing the thickness of the spacer layer) results from the charges from the donor (or equivalently from the charges from 2DEG electrons in addition to the depletion charge and back-gate contribution, considering the charge neutrality), and therefore $-d\phi/dz = (-e/\epsilon_0\epsilon)(n_{\text{depl}} + n_e - \Delta n_{\text{bg}})$. The depletion charge and the depletion layer thickness are found by the conditions $\phi(z_{\text{depl}}) = E_g/(-e)$ and $d\phi/dz(z_{\text{depl}}) = 0$, setting $\Delta n_{\text{bg}} = 0$. We obtain $n_{\text{depl}} = (2\epsilon_0\epsilon N_A E_g/e^2)^{1/2}$ and $z_{\text{depl}} = (2\epsilon_0\epsilon E_g/e^2 N_A)^{1/2}$, respectively, the latter being the order of micro meters. As a band gap of the GaAs , we adopted $E_g = 1.52$ eV, the value at 4.2 K. The solution of eqs. (6), (9), and (10) with the above boundary conditions are formally written as,

$$\phi(z) = \frac{(-e)}{\epsilon_0\epsilon} \left\{ (n_{\text{depl}} - \Delta n_{\text{bg}})z - \Theta(z) \frac{1}{2} N_A z^2 + n_e [I(z) - I(z_{\text{depl}})] \right\}, \quad (11)$$

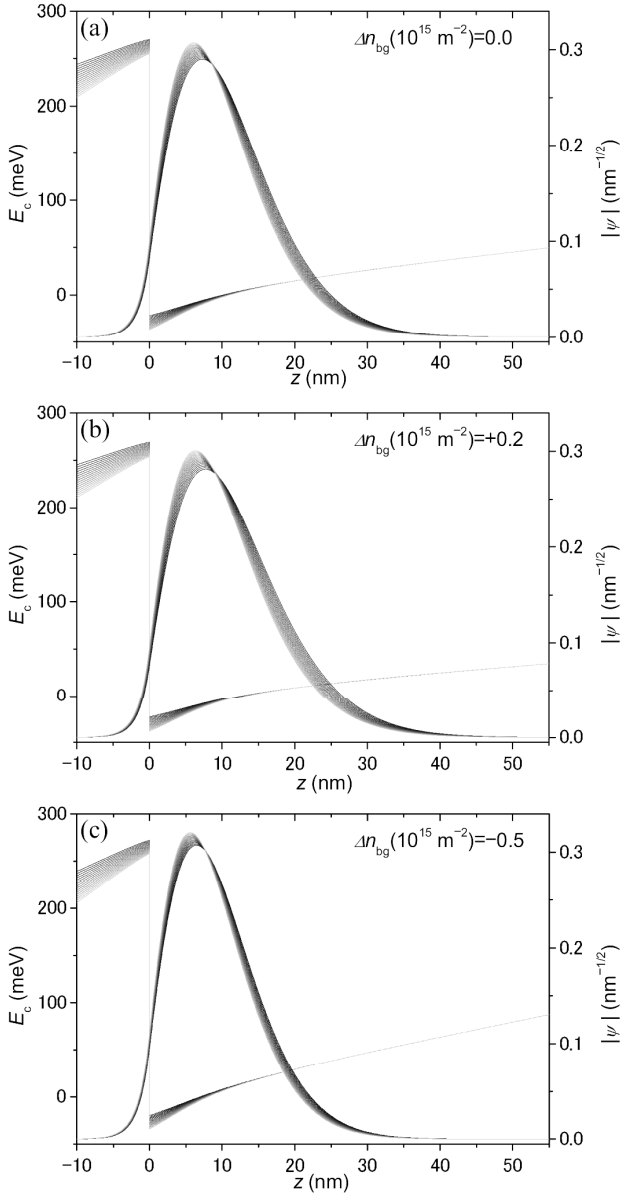


Fig. 3. Numerically calculated conduction-band edge E_c and the wave function ψ , for $N_A = 2 \times 10^{20} \text{ m}^{-3}$. The heterointerface resides at $z=0$. Calculations were done for the values of n_e (in 10^{15} m^{-2}) from 1.5 to 3.0 by the increment of 0.1 each, and displayed with progressively brighter grayscale. The back gate was set (a) neutral (Δn_{bg} (in 10^{15} m^{-2}) = 0.0) (b) positive (+0.2), and (c) negative (-0.5).

with

$$I(z) \equiv z - \int_{-\infty}^z dz' \int_{-\infty}^{z'} dz'' |\psi(z'')|^2. \quad (12)$$

Numerical solutions of the wave function $\psi(z)$, and the z dependence of the conduction-band edge E_c , which is no other than the confinement potential $V(z)$, is plotted in Fig. 3. Figure 3(a) to (c) correspond to different settings of the back-gate voltages $\Delta n_{\text{bg}} = (\epsilon_0 \epsilon / e d_{\text{bg}}) V_{\text{bg}}$. For each Δn_{bg} , calculations are repeated for different n_e 's ranging from 1.5 to $3.0 \times 10^{15} \text{ m}^{-2}$ with an increment of $0.1 \times 10^{15} \text{ m}^{-2}$ each. As a matter of course, the confinement potential, hence the wave function, becomes thicker (thinner) for a positive (negative) back-gate voltage. For

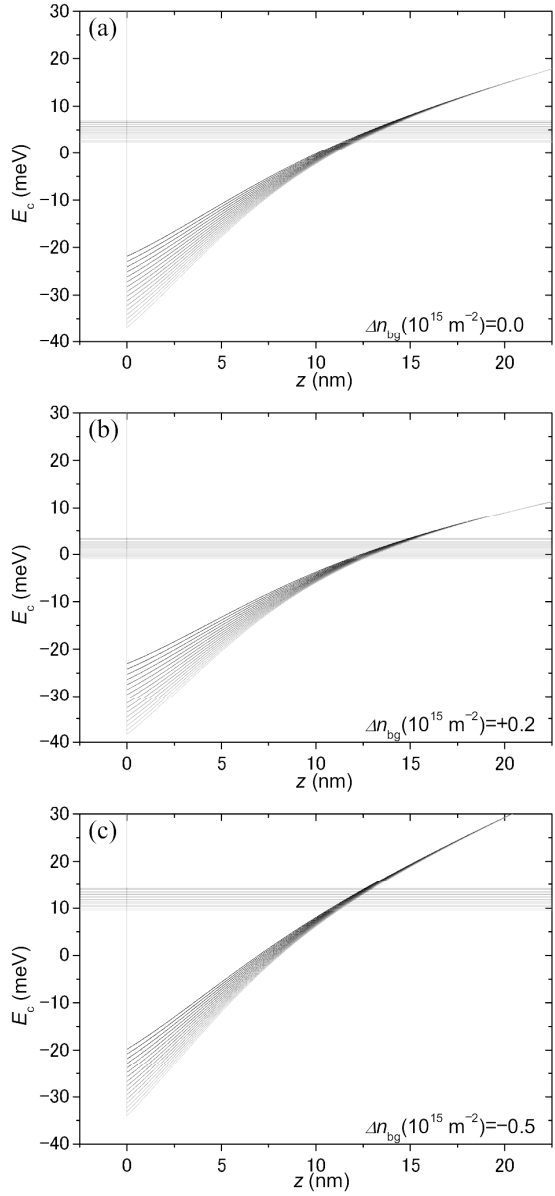


Fig. 4. The conduction-band edge E_c near the heterointerface and the lowest-subband level E_1 . The values of N_A , n_e , and Δn_{bg} , and the grayscale are the same as in Fig. 3

a fixed Δn_{bg} , the width of $\psi(z)$ decreases with increasing n_e , owing to the last term in eq. (11). The change in the thickness is more conspicuous for larger (more positive) Δn_{bg} . This is more clearly illustrated in Fig. 5(a), which plots rms thickness of the wave function versus n_e for varying settings of Δn_{bg} ranging from -0.5 to +0.2 with an interval of 0.1 (in 10^{15} m^{-2}). Figure 4 shows close-up of E_c in the proximity of the heterointerface along with the lowest subband level E_1 . The conduction-band edge E_c at the heterointerface, $z=0$, displays downward shift with the increase of n_e . Accompanying this deepening of the bottom of the confinement potential, the subband level E_1 is also displaced downward but with smaller decrement. Close inspection of Fig. 4(a)–(c) reveals that the downward shift in E_c by n_e is larger (smaller) for more positive (negative) back-gate voltages, while the extent of shift in E_1 remains virtually unchanged. E_c at

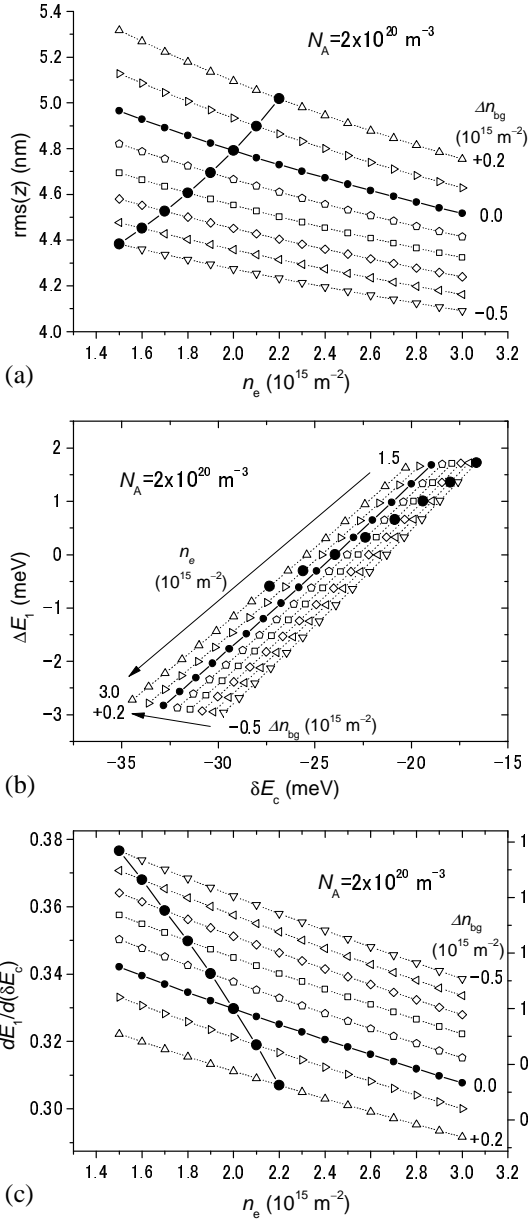


Fig. 5. (a) rms thickness of the wave function vs n_e , (b) the shift ΔE_1 of the lowest subband level E_1 (measured from the value at $n_e = 2.0 \times 10^{15} \text{ m}^{-2}$) vs the shift δE_c of the conduction-band edge just above the heterointerface, (c) the rate of the change of E_1 in response to the change in δE_c , for different settings of the back gate (Δn_{bg} from -0.5 to $+0.2 \times 10^{15} \text{ m}^{-2}$ at the interval of $0.1 \times 10^{15} \text{ m}^{-2}$, each plotted by differently shaped symbols), and $N_A = 2 \times 10^{20} \text{ m}^{-3}$. The large (small) solid circles designate how the values evolve when n_e is varied by the back gate (by illumination). The right axis in (c) shows the ratio with the value at $n_e = 2.0 \times 10^{15} \text{ m}^{-2}$ and $\Delta n_{\text{bg}} = 0.0 \times 10^{15} \text{ m}^{-2}$.

the heterointerface approximately represents the E_c just above 2DEG, the E_c that we will be looking at (to be denoted as δE_c), apart from minor modification caused by not including the contribution from the tail of the wave function in the $\text{Al}_x\text{Ga}_{1-x}\text{As}$ barrier layer and including the contribution from $V_{\text{xc}}(0)$. More quantitative account is given in Fig. 5(b).

Before explaining Fig. 5 further, we look into more detail of the behavior of the last term in eq. (11), which gov-

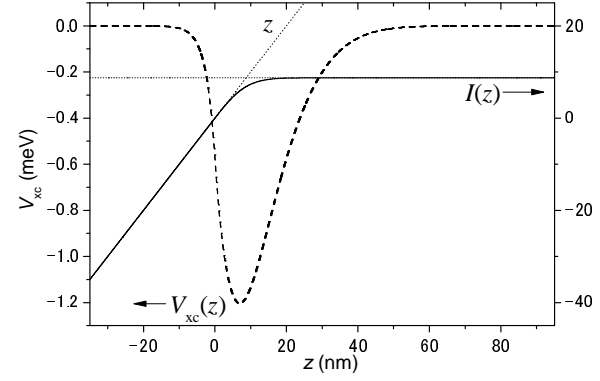


Fig. 6. $V_{\text{xc}}(z)$ (dashed curve, left axis) and $I(z)$ (solid curve, right axis) calculated for $N_A = 2 \times 10^{20} \text{ m}^{-3}$, $n_e = 2.0 \times 10^{15} \text{ m}^{-2}$, and $\Delta n_{\text{bg}} = 0.0 \times 10^{15} \text{ m}^{-2}$.

erns the n_e dependences we have just pointed out. The function $I(z)$ appearing in the term tends to z for $z \ll 0$, and to a constant value dependent on the distribution of $\psi(z)$ for large enough $z (\gg |z|)$, as exemplified in Fig. 6 for particular values of N_A , n_e , and Δn_{bg} . It can easily be perceived from the definition eq. (12) that the constant value at $z \gg |z|$, $I(\infty) [\simeq I(z_{\text{depl}})$ since $z_{\text{depl}} \gg |z|$], increases with increasing width of $\psi(z)$. Physically, this reflects the property of the solution of the Poisson's equation that the potential change across a space-charge layer with a given amount of charge is larger when the charge is spatially spread over more widely. These features are transparent for Fang-Howard wave function, which allows analytic evaluation as $I(z) = z - \Theta(z)[z - 3/b + \exp(-bz)(3 + 2bz + b^2z^2/2)/b]$ and $I(z_{\text{depl}}) \simeq I(\infty) = 3/b$.

The net shift in E_c across the 2DEG (from $z < 0$ to $z > 0$) brought about by electrons themselves is given by

$$\delta E_c = -\frac{e^2}{\epsilon_0 \epsilon} n_e I(z_{\text{depl}}), \quad (13)$$

which includes the contribution from the tail of $\psi(z)$ in the barrier layer. Although $V_{\text{xc}}(z)$ also depends on n_e , it does not contribute to the net shift since it vanishes where $\psi(z)$ vanishes (see eqs. (7), (8) and an example in Fig. 6). Note that $I(z_{\text{depl}}) = 0$ for an ideal zero-thickness 2DEG $|\psi(z)|^2 = \delta(z)$, therefore eq. (13) is the effect resulting exclusively from the finite thickness.

It is worth pointing out that the last term in eq. (11) is the only ‘‘plastic’’ term in $\phi(z)$ that can be modified externally from the front surface. All the other terms are fixed once the sample quality (N_A) and the back-gate setting (Δn_{bg}) are fixed. An attempt to introduce potential modulation from the surface, e.g., by the grating induces perturbing spatial variation in E_c above the 2DEG, namely, in δE_c . Following the change in $\delta E_c(\mathbf{r})$ at the position \mathbf{r} in the x - y plane, $n_e(\mathbf{r})$, $\psi(\mathbf{r}, z)$, and hence $E_1(\mathbf{r})$ are also slightly altered to fulfill eqs. (6), (9), (10) and (13) with the modified δE_c , thereby resulting in the spatial variation in E_1 . When the modulation amplitude is small enough, as is the case in the present study, the conversion ratio from δE_c to E_1 can be evaluated by the derivative $dE_1/d(\delta E_c)$ at the original n_e . Further, with a plausible assumption that the amplitude of the variation in δE_c to be introduced from the surface does not

depend on properties at and below 2DEG, i.e., on n_e , n_{depl} , and Δn_{bg} , the amplitude V_0 seen by electrons will be proportional to $dE_1/d(\delta E_c)$.

In Fig. 5(b), E_1 is plotted against δE_c given by eq. (13). (To plot all of them within a single frame, E_1 's are negatively offset by the value at $n_e=2.0 \times 10^{15} \text{ m}^{-2}$ for each Δn_{bg} , hence the notation ΔE_1 .) The plots are for the same sets of n_e and Δn_{bg} as in (a). Applying external perturbation to introduce modulation corresponds to slightly shifting the point $(\delta E_c, \Delta E_1)$ along the curve of constant Δn_{bg} , because the perturbation is assumed not to affect Δn_{bg} . Therefore the slope of the constant Δn_{bg} curve is the $dE_1/d(\delta E_c)$ to be considered here. It can be seen in Fig. 5(b) and clearer in Fig. 5(c), which plots²⁶ $dE_1/d(\delta E_c)$ versus n_e , that the slope has a trend of becoming smaller with increasing n_e if Δn_{bg} is kept constant, and also with increasing (more positive) Δn_{bg} . It is to this trend that we ascribe the observed behavior of V_0 . The decrease of $dE_1/d(\delta E_c)$ by increasing Δn_{bg} is readily interpretable as an effect of the thickness of the 2DEG: the negative shift of δE_c with n_e is more rapid for thicker 2DEG while the decrease in E_1 does not change very much (see Fig. 4 or Fig. 5(b)), and therefore $dE_1/d(\delta E_c)$ is smaller for thicker 2DEG. The decrease of $dE_1/d(\delta E_c)$ with increasing n_e for constant Δn_{bg} originates from more subtle competition between the shift in δE_c and E_1 : both shift downward with increasing n_e , and the rate of the shift decreases with increasing n_e whose rate (the rate of ‘‘the rate of shift’’) decelerating slightly more rapidly for δE_c , leaving the rate of change for δE_c relatively larger than that of E_1 .

In Fig. 5, the results of the calculations are plotted for all possible sets of n_e and Δn_{bg} . In the experiment, n_e was varied either by the back gate alone, namely $n_e = n_{e0} + \Delta n_{\text{bg}}$ with n_{e0} fixed, or by illumination with the back-gate voltage fixed to zero $\Delta n_{\text{bg}} = 0$. The plotted points corresponding to the two experimental modes are highlighted by large and small solid circles, respectively, with n_{e0} set to $2.0 \times 10^{15} \text{ m}^{-2}$. Figure 5(a) shows that rms thickness increases with increasing n_e when varied by the back gate, while the trend is reversed when n_e is varied by illumination. As demonstrated in Fig. 5(c), on the other hand, $dE_1/d(\delta E_c)$ decreases for both methods with the rate of the change much larger when n_e is driven by the back gate. Thus, $dE_1/d(\delta E_c)$ behaves in qualitatively the same manner as V_0 under the variation of n_e by the back gate and by illumination.

To see how N_A affects the problem, we calculate $dE_1/d(\delta E_c)$ for two other values of N_A through the same procedure as was done for Fig. 5(c), and plot in Fig. 7 the $dE_1/d(\delta E_c)$ normalized by its value at $n_e = 2.0 \times 10^{15} \text{ m}^{-2}$. The figure shows that the behavior does not depend very much on N_A when n_e is varied by illumination, while the value of N_A has strong impact on the rate of decrease when the back gate is in use; the decrease is more rapid for smaller N_A , i.e., for cleaner 2DEG. This is readily interpretable in terms of its effect on the confinement potential. As manifest from eq. (11), the confinement potential has the same profile as long as $n'_{\text{depl}} = n_{\text{depl}} - \Delta n_{\text{bg}}$, which should be positive for the confinement to be operative, remains unchanged. Small N_A hence small n_{depl}

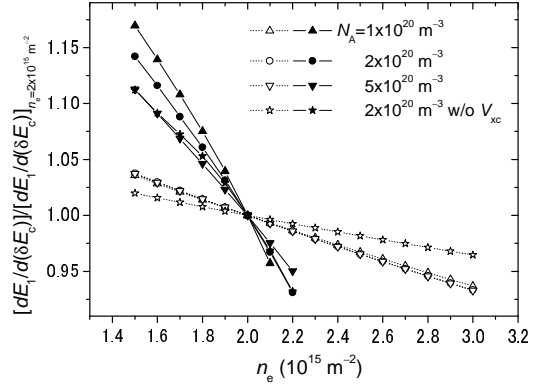


Fig. 7. The rate of change $dE_1/d(\delta E_c)$ (normalized by the value at $n_e = 2.0 \times 10^{15} \text{ m}^{-2}$ and $\Delta n_{\text{bg}} = 0.0 \times 10^{15} \text{ m}^{-2}$) plotted as a function of n_e for different values of N_A . Solid and open symbols correspond to varying n_e by the back gate and by illumination, respectively. Stars represent the calculation without $V_{\text{xc}}(z)$ in eq. (6).

intensifies the relative importance of the variation of the Δn_{bg} . Large solid circles in Fig. 5(c) shows that the rate of the change of $dE_1/d(\delta E_c)$ versus n_e , varied by the back gate, increases with increasing (more positive) Δn_{bg} , namely, with increasing thickness of the 2DEG. Since decreasing n_{depl} is equivalent to increasing Δn_{bg} , it also adds to the change rate. The qualitative behavior of $dE_1/d(\delta E_c)$ under the variation of n_e , N_A , and Δn_{bg} is reproduced in a simple analytic calculation using Fang-Howard wave function (see Appendix).

For quantitative comparison with the experiment, the plots in Fig. 7 for $N_A = 1.0$ and $2.0 \times 10^{20} \text{ m}^{-3}$ are replotted in Fig. 2(b).²⁷ As mentioned before, the rationale of comparing V_0 with $dE_1/d(\delta E_c)$ is given by the assumption that the amplitude of the periodic modulation in δE_c is determined solely by the grating on the surface and independent of n_e , N_A , and Δn_{bg} ; from the assumption, the proportionality of V_0 and $dE_1/d(\delta E_c)$ is expected to result. (Note, however, that it is only the proportionality that can be compared with experiment, since we currently do not have a method to directly measure the amplitude of the modulation of δE_c .) Fig. 2(b) demonstrates that the behavior of V_0 under back gate and illumination is explained by that of $dE_1/d(\delta E_c)$ fairly well. The agreement is better for $N_A = 1.0 \times 10^{20} \text{ m}^{-3}$, implying that the density of residual impurity in our 2DEG wafer may be closer to this value (or smaller). However, since we have used simplified model for the confinement potential, and have neglected many complications, e.g., possible screening by the Si-doped layer,²⁸ it seems going too far to use this comparison for quantitatively accurate determination of N_A .

Finally, we discuss the effect of the exchange and correlation term $V_{\text{xc}}(z)$. In Fig. 7 we also plot the result of calculation deliberately omitting the term $V_{\text{xc}}(z)$ from eq. (6). The plot, along with Fig. 2(b), illustrates that experiments are better described with inclusion of $V_{\text{xc}}(z)$. The predominant effect of $V_{\text{xc}}(z)$ is twofold: it reduces the thickness of the 2DEG hence the downward shift of δE_c , and also reduces E_1 by partially alleviating the penalty

in energy due to the Hartree term. It turns out by examining the process of the calculation that the decrease in E_1 by $V_{xc}(z)$ dominates the difference with and without the term. The effect is more pronounced for larger n_e , letting the decrease of $dE_1/d(\delta E_c)$ with n_e more rapid and closer to the experiment. This underlines the importance of the exchange-correlation effect, albeit the smallness of its magnitude, in understanding the behavior of the potential modulation in the 2DEG.

5. Conclusions

We have reported our experimental result that the amplitude V_0 of potential modulation decreases with increasing electron density n_e , varied either by the back gate or by illumination. Contrary to the intuition, the decrease is much more rapid when the back gate is employed. We have ascribed the result to the modification in the conversion rate $dE_1/d(\delta E_c)$ for the perturbing modulation with its source at the surface (or more generally, above the 2DEG) to be transmitted to the subband level in the confinement potential $V(z)$. The origin of the substantial change in $dE_1/d(\delta E_c)$ can be traced back to the high sensitivity, particularly notable in a SH 2DEG, of the profile of $V(z)$ hence of the envelope function $\psi(z)$ to the change in the electron density or the back-gate setting. Therefore we expect much smaller effect in a 2DEG formed in a single quantum well. The present result provides a prescription for making the modulation amplitude large in SH 2DEG; that is, it is advantageous to make the 2DEG as thin as possible. This is especially important for a small period ULSL for which the amplitude becomes inevitably small.

Although we have in the present paper confined our interest to ULSL, for which the measurement of the modulation amplitude V_0 is possible, the decrease of V_0 with increasing n_e will also take place likewise in other low-dimensional electron systems based on SH 2DEG with potential modulation. Moreover, even in plain SH 2DEGs without any artificial modulation, the random potential landscape seen by electrons, since its main source is ionized donors located *above* the 2DEG, will diminish its amplitude with increasing n_e . The effect should be born in mind in interpreting the experiment with variation of n_e , especially when n_e is varied by the back gate.^{15, 29, 30}

Acknowledgment

This work was supported by Grant-in-Aid for Scientific Research (C) (15540305) and (A) (13304025) and Grant-in-Aid for COE Research (12CE2004) from Ministry of Education, Culture, Sports, Science and Technology.

Appendix: Fang-Howard approximation

The Fang-Howard approximation, although not quantitatively quite accurate, provides analytic formula, which will be useful for the qualitative understanding of the phenomenon. Here, we calculate $dE_1/d(\delta E_c)$ using Fang-Howard wave function $\psi_{\text{FH}}(z)$. The lowest subband energy is given by the sum of the expectation values of the kinetic energy and the potential energy, $E_1 = \langle T \rangle + \langle V \rangle$, with $\langle T \rangle = \langle \psi_{\text{FH}}(z) | (-\hbar^2/2m^*) (d^2/dz^2) | \psi_{\text{FH}}(z) \rangle = \hbar^2 b^2 / 8m^*$.

In evaluating potential energy, we neglect $V_{xc}(z)$ for simplicity. Noting that $\psi_{\text{FH}}(z)$ vanishes at $z < 0$, we obtain, using eq. (11),

$$\begin{aligned} \langle V \rangle &= \langle \psi_{\text{FH}}(z) | (-e)\phi(z) | \psi_{\text{FH}}(z) \rangle \\ &= \frac{3e^2}{\epsilon_0\epsilon} \left(\frac{n_{\text{depl}} - \Delta n_{\text{bg}} - 5n_e/16}{b} - \frac{2N_A}{b^2} \right), \end{aligned} \quad (\text{A.1})$$

thus,

$$\begin{aligned} E_1 &= \text{Ry}^* \left[\frac{1}{4} a_B^*{}^2 b^2 \right. \\ &\quad \left. + 24\pi a_B^* \left(\frac{n'_{\text{depl}} - 5n_e/16}{b} - \frac{2N_A}{b^2} \right) \right], \end{aligned} \quad (\text{A.2})$$

with $n'_{\text{depl}} \equiv n_{\text{depl}} - \Delta n_{\text{bg}}$. As mentioned before,

$$\delta E_c = -\frac{e^2}{\epsilon_0\epsilon} n_e \frac{3}{b} = -24\pi \text{Ry}^* a_B^* n_e \frac{1}{b}. \quad (\text{A.3})$$

Making use of the relation^{16, 31} $b = [48\pi(n'_{\text{depl}} + 11n_e/32)/a_B^*]^{1/3}$, and being reminded that N_A hence n_{depl} , and Δn_{bg} are fixed, b can be made the only free parameter by eliminating n_e , and therefore,

$$\begin{aligned} \frac{dE_1}{d(\delta E_c)} &= \frac{dE_1/db}{d(\delta E_c)/db} \\ &= \frac{(3a_B^*/16\pi)b^3 + 21n'_{\text{depl}} - 44N_A/b}{(4a_B^*/3\pi)b^3 + 32n'_{\text{depl}}} \\ &= \frac{5}{16} \left[\frac{n'_{\text{depl}} + (33/320)n_e - (22/15)N_A/b}{n'_{\text{depl}} + (11/48)n_e} \right]. \end{aligned} \quad (\text{A.4})$$

In the last equality, the parameter b is replaced back again to n_e , except for the term including N_A , which is negligibly (roughly three orders of magnitude) small compared with other terms. It is easy to verify from eq. (A.4) that $dE_1/d(\delta E_c)$ decreases with increasing n_e when (i) $n_{e0} \equiv n_e - \Delta n_{\text{bg}}$ is fixed (simulating the back-gate control) and (ii) n'_{depl} is kept constant (simulating the illumination), and the rate of change is larger for the former.

- 1) C. W. J. Beenakker and H. van Houten: *Solid State Physics*, eds. H. Ehrenreich and D. Turnbull, (Academic Press, San Diego, 1991) p. 1.
- 2) D. Weiss, K. v. Klitzing, K. Ploog and G. Weimann: *Europhys. Lett.* **8** (1989) 179.
- 3) The fractional quantum Hall effect is a typical example. See, e.g., K. Park, N. Meskini and J. K. Jain: *J. Phys.: Condens. Matter* **11** (1999) 7283.
- 4) E. Skuras, A. R. Long, I. A. Larkin, J. H. Davies and M. C. Holland: *Appl. Phys. Lett.* **70** (1997) 871.
- 5) J. Fujita and Y. Ohnishi and Y. Ochiai and S. Matsui: *Appl. Phys. Lett.* **68** (1996) 1297.
- 6) A. Endo, S. Katsumoto and Y. Iye: *Phys. Rev. B* **62** (2000) 16761.
- 7) The electron density slightly ($\leq 5\%$) decreases on depositing the back gate even when $V_{\text{bg}}=0$. This is attributable to the large work function of gold, which effectively work as natively negative voltage.
- 8) P. H. Beton, E. S. Alves, P. C. Main, L. Eaves, M. W. Dellow, M. Henini, O. H. Hughes, S. P. Beaumont and C. D. W. Wilkinson: *Phys. Rev. B* **42** (1990) R9229.

- 9) Higher order harmonics are neglected throughout this paper. A quantitative account of higher-harmonic contents will be presented elsewhere.
- 10) C. W. J. Beenakker: Phys. Rev. Lett. **62** (1989) 2020.
- 11) F. M. Peeters and P. Vasilopoulos: Phys. Rev. B **46** (1992) 4667.
- 12) P. T. Coleridge: Phys. Rev. B **44** (1991) 3793.
- 13) A. Endo and Y. Iye: in preparation.
- 14) This is in accordance with the simple electrostatics that predicts potential modulation originating at the surface to decay as $\propto \exp(-2\pi d/a)$, where d is the depth of the 2DEG plane from the surface (90 nm plus the average thickness of the 2DEG). Dependence of V_0 on a will be reported in detail elsewhere, A. Endo and Y. Iye: in preparation.
- 15) A. Soibel, U. Meriav, D. Mahalu and H. Shtrikman: Phys. Rev. B **55** (1997) 4482.
- 16) T. Ando, A. B. Fowler and F. Stern: Rev. Mod. Phys. **54** (1982) 437.
- 17) J. H. Davies: *The Physics of Low-dimensional Semiconductors* (Cambridge University Press, 1998).
- 18) P. J. Price: Surf. Sci. **143** (1984) 145.
- 19) K. Hirakawa and H. Sakaki: Phys. Rev. B **33** (1986) 8291.
- 20) K. Esfarjani and H. R. Glyde: Phys. Rev. B **41** (1990) 1042.
- 21) F. F. Fang and W. E. Howard: Phys. Rev. Lett. **16** (1966) 797.
- 22) T. Ando: J. Phys. Soc. Jpn. **51** (1982) 3893.
- 23) F. Stern and S. Das Sarma: Phys. Rev. B **30** (1984) 840.
- 24) L. Hedin and B. I. Lundqvist: J. Phys. C: Solid St. Phys. **4** (1971) 2064.
- 25) In reality, because it contains more reactive element Al, $\text{Al}_x\text{Ga}_{1-x}\text{As}$ is expected to include impurities at higher concentration than GaAs. However, N_A is important only to determine n_{depl} by the boundary condition deep inside the substrate. The direct effect of N_A near the interface is negligibly small. Therefore neglecting the background impurities in the $\text{Al}_x\text{Ga}_{1-x}\text{As}$ layer is legitimate.
- 26) The differentiation is actually performed on a quadratic polynomial fitted to the discrete points in Fig. 5(b).
- 27) Strictly, quadratic polynomials fitted to the discrete points in Fig. 7 are plotted to make the comparison with the experimental plots easy to see.
- 28) J. H. Davies and I. A. Larkin: Phys. Rev. B **49** (1994) 4800.
- 29) A. Endo and Y. Iye: Physica E **22** (2004) 122.
- 30) See, e.g., V. J. Goldman and B. Su: Science **267** (1995) 1010.
- 31) The parameter b is optimized by minimizing the energy slightly different from E_1 given in eq. (A.2) in the calculation of $\langle V \rangle$. Namely, (i) the Hartree term, resulting from the term containing $n_e I(z)$ in eq. (11), is halved to avoid double count of the electron-electron interaction,¹⁶ (ii) the term from the final term including $n_e I(z_{\text{depl}})$ in eq. (11), which was necessary to conform the boundary condition at $z=z_{\text{depl}} \gg 0$, is omitted, and (iii) the term including N_A is neglected because of its smallness.